UC San Diego
UC San Diego Previously Published Works

Title

In Situ Gene Therapy via AAV-CRISPR-Cas9-Mediated Targeted Gene Regulation

Permalink

Journal

ISSN

Authors

Moreno, Ana M
Fu, Xin
Zhu, Jie
et al.

Publication Date

DOI

Peer reviewed

In Situ Gene Therapy via AAV-CRISPR-Cas9-Mediated Targeted Gene Regulation

Ana M. Moreno,[1] Xin Fu,[2,3] Jie Zhu,[2,3] Dhruva Katrekar,[1] Yu-Ru V. Shih,[1] John Marlett,[4] Jessica Cabotaje,[1] Jasmine Tat,[1] John Naughton,[4] Leszek Lisowski,[5,6] Shyni Varghese,[1,7] Kang Zhang,[2,3,8] and Prashant Mali[1]

[1]Department of Bioengineering, University of California, San Diego, San Diego, CA, USA; [2]Shiley Eye Institute, Institute for Engineering in Medicine, Institute for Genomics Medicine, University of California, San Diego, San Diego, CA, USA; [3]Guangzhou Women and Children's Medical Center, Guangzhou Medical University, Guangzhou, China; [4]Salk Institute for Biological Studies, La Jolla, CA, USA; [5]Translational Vectorology Group, Children's Medical Research Institute, University of Sydney, Sydney, NSW 2006, Australia; [6]Military Institute of Hygiene and Epidemiology, The Biological Threats Identification and Countermeasure Centre, 24-100 Puławy, Poland; [7]Department of Biomedical Engineering, Duke University, Durham, NC, USA; [8]Veterans Administration Healthcare System, San Diego, CA, USA

Development of efficacious *in vivo* delivery platforms for CRISPR-Cas9-based epigenome engineering will be critical to enable the ability to target human diseases without permanent modification of the genome. Toward this, we utilized split-Cas9 systems to develop a modular adeno-associated viral (AAV) vector platform for CRISPR-Cas9 delivery to enable the full spectrum of targeted *in situ* gene regulation functionalities, demonstrating robust transcriptional repression (up to 80%) and activation (up to 6-fold) of target genes in cell culture and mice. We also applied our platform for targeted *in vivo* gene-repression-mediated gene therapy for retinitis pigmentosa. Specifically, we engineered targeted repression of *Nrl*, a master regulator of rod photoreceptor determination, and demonstrated *Nrl* knockdown mediates *in situ* reprogramming of rod cells into cone-like cells that are resistant to retinitis pigmentosa-specific mutations, with concomitant prevention of secondary cone loss. Furthermore, we benchmarked our results from *Nrl* knockdown with those from *in vivo* Nrl knockout via gene editing. Taken together, our AAV-CRISPR-Cas9 platform for *in vivo* epigenome engineering enables a robust approach to target disease in a genomically scarless and potentially reversible manner.

INTRODUCTION

The recent advent of RNA-guided effectors derived from CRISPR-Cas systems has transformed our ability to engineer genomes.[1–11] In addition to gene editing, CRISPR-Cas9 can also be utilized for transcriptional regulation, in which catalytically inactivated "dead" Cas9 (dCas9) can be fused to transcriptional effectors to activate or repress gene expression.[12–16] Applications of these systems for gene therapy, coupled with the growing knowledge of the genetic and pathogenic basis of disease, are likely to have great impact.

Realizing the full potential for CRISPR-based *in situ* genome and epigenome engineering entails the development of corresponding safe and efficient gene transfer platforms. In this regard, a range of novel viral- and non-viral-based approaches have been developed for *in vitro* and *in vivo* delivery of CRISPRs.[17–26] Here, we develop a CRISPR delivery platform using adeno-associated viruses (AAVs), because they are the preferred vectors for gene transfer due to their mild immune response, low toxicity, long-term transgene expression, and favorable safety profile.[27,28] Although advantageous as delivery vectors, AAVs suffer from a limited packaging capacity (∼4.7 kb). This limited capacity does not typically accommodate the payload requirements of delivering a dCas9, the associated guide RNA (gRNA), and also dCas9-fused effector domains for epigenome engineering. To overcome this limitation, utilizing recent split-Cas9 systems that use two AAV vectors for CRISPR-Cas9 delivery,[29–32] we leveraged the resulting packaging capacity in each to engineer and optimize a broader range of genome regulation functionalities, including multiplex targeting via single or dual-gRNA delivery.

We applied this system to target retinitis pigmentosa in a mouse model of the disease. Retinitis pigmentosa is an inherited retinal dystrophy affecting ∼1 in every 4,000 individuals in the general population and is characterized by progressive degeneration of rod photoreceptor cells in the retina, followed by deterioration and death of cone photoreceptor cells.[33,34] Affected patients with retinitis pigmentosa bear mutations in over 200 causative genes,[35] which limits the potential effectiveness of conventional gene therapy strategies. Additionally, targeted gene repair typically relies on endogenous homologous recombination machinery, which is usually diminished in activity in post-mitotic cells. Correspondingly, in this study, we

utilized a therapeutic *in situ* cellular reprogramming strategy to overcome these challenges in both gene therapy and endogenous tissue regeneration by aiming to switch a mutation-sensitive cell type to a functionally related cell type resistant to that mutation. Specifically, we targeted *Nrl*, a master regulator of rod versus cone photoreceptor determination, which activates *Nr2e3*, a transcription factor that represses transcription of multiple cone-specific genes.[36] Consistent with this, transgenic strategies in mice have demonstrated that knockdown of rod photoreceptor determinant *Nrl* in adult rod cells results in reprogramming of rods into cone-like cells resistant to rod photoreceptor retinitis pigmentosa-specific mutations, with prevention of secondary cone loss.[35] Recent work has also demonstrated that, in adult rod cells, *in situ* genome editing of rod photoreceptor determinant *Nrl* results in reprogramming of rods into cone-like cells that are resistant to rod photoreceptor retinitis pigmentosa-specific mutations, as well as prevention of secondary cone loss.[37,38] Building on these studies, we conducted targeted *in situ Nrl* gene repression in the mouse retina to determine whether we could reprogram rods into cone-like cells in a genomically scarless manner. We also benchmarked these results with those obtained via Cas9-based gene editing of *Nrl*.

RESULTS

In Vitro and *In Vivo* Genome Editing via a Dual-AAV Split-Cas9 System

We first confirmed that split-Cas9 constructs delivered as AAVs were functional *in vitro* and *in vivo*. Expression cassettes of split-*Streptococcus pyogenes* (SpCas9) and gRNA were delivered via a dual-AAV vector system (Figure S1A). The first AAV contains a gRNA driven by a human RNA polymerase III promoter, U6, and a N-terminal Cas9 (NCas9) fused to an N-intein driven by a cytomegalovirus (CMV) promoter, as well as a polyadenylation (polyA) signal.[30] The second AAV cassette contains a CMV-driven C-terminal Cas9 (CCas9) fused to a C-intein as well as a polyA signal. We confirmed targeted genome editing through next-generation sequencing (NGS)[40] across two distinct cell types *in vitro* (Figure S1C), notably also observing robust AAV6-mediated editing in human CD34+ hematopoietic stem cells. We additionally confirmed *in vivo* genome editing in adult C57BL/6J mice injected with 5E+11 vg/split-Cas9/mouse through the tail vein (Figure S1C).

As a hit and run approach suffices for genome editing and is preferable over long-term nuclease expression, we next engineered small-molecule inducibility[32,41,42] of *in vivo* CRISPR-Cas9 editing activity. Specifically, we engineered one AAV construct to bear a minimal CMV promoter with a tetracycline response element (TRE) upstream of the C-intein-CCas9 fusion, whereas the other bore a full-length CMV promoter that drives expression of the N-intein-NCas9 fusion and a tet-regulatable activator (tetA). The binding of tetA to the TRE, upon doxycycline addition, allows for inducible expression of the CCas9 and thereby temporal regulation of genome editing (Figure S1B). We confirmed robust functioning of this system both *in vitro* and *in vivo* (Figures S1D and S1E). Taken together, these

studies confirmed the functionality of the dual-AAV split-Cas9 format for CRISPR-Cas9 delivery.

In Vitro and *In Vivo* Genome Regulation via a Dual-AAV Split-dCas9 System

Next, to engineer targeted genome repression and activation, we utilized a dead split-Cas9 (dCas9) protein and its fusion to repression and activation domains (specifically a KRAB and a VP64+rTA [VR] domain, respectively; Figures 1A and 1B).[12–16] Utilizing the dual-AAV strategy enabled us to package these additional effector domains without exceeding the viral packaging capacity. We confirmed functionality via *in vitro* experiments in HEK293T cells targeting *CXCR4* for repression and *RHOX1* for activation utilizing the AAV-DJ serotype, with control non-targeting virus (equal viral titers). For *in vivo* AAV delivery, we performed tail vein injections at titers of 5E+11 vg/split-dCas9/mouse using the AAV8 serotype and harvested mice livers 4 weeks post-injection. We achieved 80% *in vivo* repression at the *Cd81* locus (n = 4; p < 0.0001) and over 2-fold *in vivo* activation at the *Afp* locus (n = 4; p = 0.0117). Taken together, we confirmed targeted gene repression and activation, as assayed via qRT-PCR, in both *in vitro* and *in vivo* scenarios and across multiple genomic loci (Figures 1C–1F).

To see whether we could further improve targeted genome regulation, we screened additional repression and activation domains by taking advantage of the modular vector designs of our dual-AAV-CRISPR platform (Figure 2A). Specifically, for our activation system, we evaluated coupling of additional VP64 or P65 domains onto the N-terminal of the dCas9 vector (dNCas9). The additional domains indeed yielded enhanced activation of a target locus (*ASCL1*) in HEK293T cells, with a ~17-fold higher activation with VP64 (n = 3; p = 0.0387) and ~23-fold higher activation with P65 (n = 3; p = 0.0069; Figure 2B), implying that tethering of a VP64 or P65 domain on the N-terminal in addition to the existing VP64-RTA on the C-terminal led to improved gene activation. We further confirmed this improved architecture *in vivo* in mice, observing over 6-fold activation at the *Afp* locus (n = 4; p = 0.0271; Figure 2B). In addition, to evaluate the *in vivo* kinetics of CRISPR-based gene regulation, we performed a time course ELISA on mice injected with 5E+11 vg/split-dCas9/mouse of AAV8 VP64-dCas9-VR-Afp, which were bled weekly for 10 weeks. Control mice received equal titers of a non-targeting AAV8 virus. We observed that *Afp* activation peaks at week 6, with a 19 ng/mL concentration of *Afp* in the blood, from a baseline of 3.8 ng/mL (calculated based on an *Afp* protein standard curve; Figure 2C).

Next, we focused on optimizing targeted gene repression. Whereas dCas9 alone can cause repression, as it can halt RNA polymerase progression by steric hindrance when targeted downstream of the transcription start site (TSS), or can competitively interfere with transcription factor binding when targeted to promoter regions or regulatory elements,[12,44,45] KRAB-dCas9 has been shown to be more potent for gene silencing than dCas9 alone.[45–47] To determine whether we could further improve the repression system, we
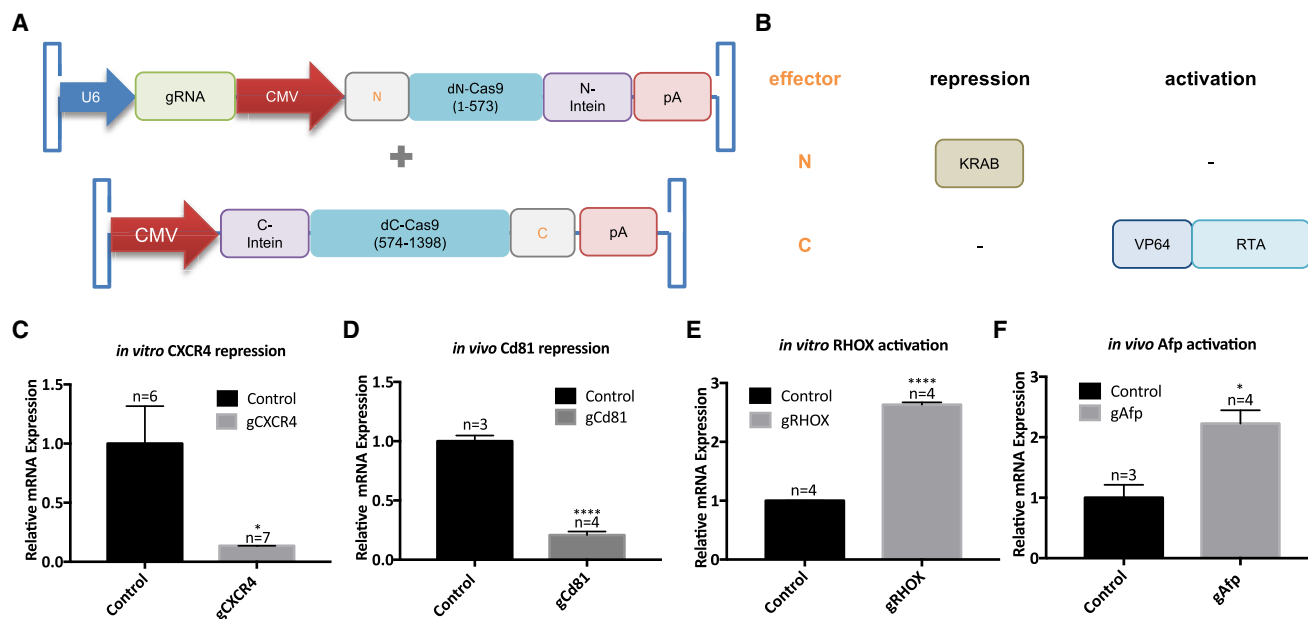
Figure 1. Versatile Genome Regulation via a Modular Dual-AAV Split-dCas9 System

(A) Schematic of intein-mediated split-dCas9 pAAVs for genome regulation. (B) Approach for modular usage of effector cassettes to enable genome repression via a KRAB-dCas9 repressor fusion protein and genome activation via a dCas9-VP64-RTA fusion protein is shown. (C) *In vitro CXCR4* repression in HEK293T cells utilizing two spacers targeting the *CXCR4* locus, as determined by qRT-PCR is shown. Controls consist of a gRNA targeting the *AAVS1* locus. (n = 3; error bars are SEM; Student's t test; p = 0.0127). (D) *In vivo Cd81* repression in adult mice livers utilizing two spacers targeting the *Cd81* locus, as determined by qRT-PCR, is shown. Control mice received non-targeting AAV8 virus at the same titers, 5E+11 vg/split-dCas9/mouse. (n = 4; error bars are SEM; Student's t test; p < 0.0001). (E) *In vitro RHOX* activation in HEK293T cells utilizing two spacers targeting the *RHOX* locus, as determined by qRT-PCR, is shown. Controls consist of a gRNA targeting the *AAVS1* locus. (n = 3; error bars are SEM; Student's t test; p < 0.0001). (F) *In vivo Afp* activation in adult mice livers utilizing two spacers targeting *Afp* locus, as determined by qRT-PCR, is shown. Control mice received non-targeting AAV8 virus at the same titers, 5E+11 vg/split-dCas9/mouse. (n = 4; error bars are SEM; Student's t test; p = 0.0117). *p ≤ 0.05; ****p ≤ 0.0001.

evaluated fusions of additional KRAB, DNA methyltransferase domains (DNMT3A or DNMT3L),[48,49] or FOG1[50] onto the C-terminal of the dCas9 vector (dCCas9) and also the use of single versus dual-gRNAs. To avoid repeat sequences in the AAV that can compromise vector stability and viral titers, we utilized a human U6 promoter and a mouse U6 promoter to drive each individual gRNA and also used non-homologous *trans*-activating small RNA (tracrRNA) sequences.[51] However, we did not observe an increase in repression with the addition of repression domains, implying that a single KRAB domain suffices for our transient repression assays in HEK293T cells, but the use of dual-gRNAs consistently yielded enhanced gene repression (Figures 2D and S2).

In Situ Cellular Reprogramming of Rod Photoreceptors

Having established a robust *in vivo* genome regulation system, we next focused on applying the same in a therapeutically relevant mouse model of disease, specifically focusing on retinitis pigmentosa. For these studies, we utilized an AAV2 mutant containing a tyrosine to phenylalanine substitution (Y444F) due to its high retinal transduction efficiency.[52] To further boost gene targeting, we utilized a dual-gRNA approach per above. We designed corresponding Cas9-based editing (split-Cas9-Nrl) and dCas9-based repression system (split-KRAB-dCas9-Nrl), where the KRAB repressor domain is fused to the N-terminal of the dCas9 protein (Figures 3A–3C). We first delivered the split-Cas9-Nrl vectors into mouse embryonic fibroblasts (MEFs) and assessed gene editing rates through a T7E1 assay, which cuts mismatched double-stranded DNA (dsDNA), and confirmed editing rates of about ~25% (Figure S3A).

We next used qRT-PCR to measure the relative expression levels of photoreceptor-specific genes in reprogrammed retinas and controls. We confirmed downregulation of *Nrl*, with simultaneous upregulation of cone-specific genes, i.e., *Arr3*, *Opnlmw*, *PDE6C*, and *GNAT2* (Figure S3B). To assay rod reprogramming into cone-like cells, we transduced transgenic Nrl-EGFP mice bearing GFP-labeled rod photoreceptor cells, with 2E+10 vg/split-Cas9/mouse of AAV-split-Cas9 or 2E+10 vg/split-dCas9/mouse of AAV-split-KRAB-dCas9 systems targeting *Nrl* into the subretinal space at postnatal day 7 (P7). These were then sacrificed for histology at P30 via flash freezing, sectioning, and staining of retinas for a cone marker, cone arrestin (mCAR). We indeed observed a reprogrammed photoreceptor phenotype with both our split-Cas9-Nrl and split-KRAB-dCas9-Nrl *in vivo*, with a decrease in Nrl-GFP+ rod photoreceptors (Figure S3C) and an increase in the number of mCAR-positive cells (Figure S3D). We next repeated the above experiments in normal wild-type C57BL6 mice. Consistent with the results in Nrl-EGFP transgenic mice, we again observed a reprogrammed photoreceptor phenotype in the retina, characterized by a significant increase in the number of
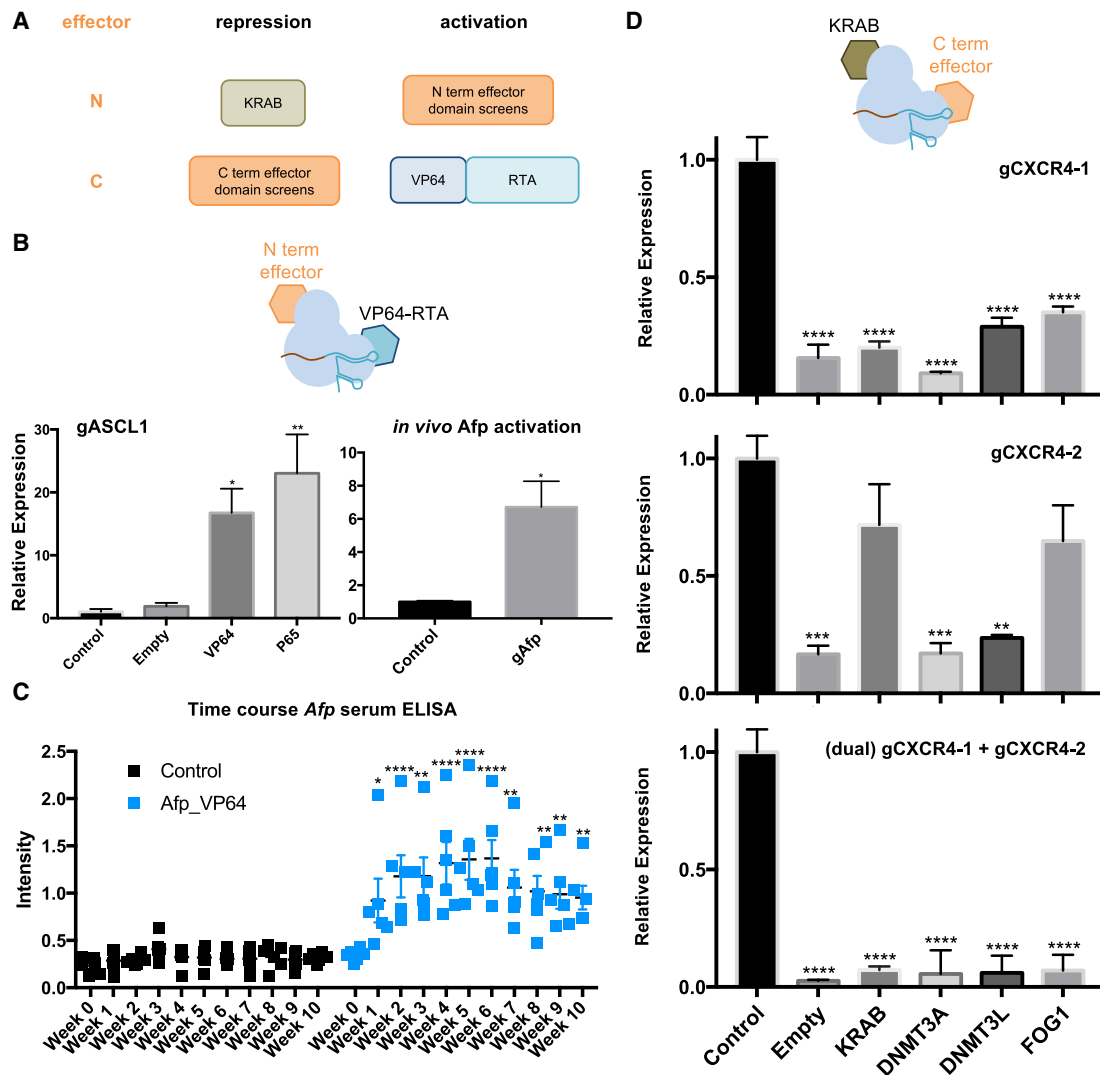
Figure 2. Domain Optimization for AAV-CRISPR Regulation

(A) Taking advantage of the extra space in the split-dCas9 system, additional activation domains were fused onto the C-terminal and additional repression domains were fused onto the N-terminal. (B) Domain optimization for AAV-CRISPR activation (left panel) is shown: activity of multiple N-terminal domain fusions: VP64 and P65 were evaluated, and notably, addition of a VP64 domain yielded ∼17-fold higher gene expression and addition of P65 yielded ∼23-fold higher expression after transfection. (n = 3; error bars are SEM; one-way ANOVA; p = 0.0387 and p = 0.0069, respectively; HEK293T cells; locus: *ASCL1*). Based on this, a VP64 activation domain was added onto the dNCas9 vector, and the *in vivo Afp* activation experiments were repeated in mice (right panel) receiving 5E+11 vg/split-dCas9/mouse of AAV8 split-VP64-dCas9-VR-Afp. Control mice received non-targeting AAV8 virus at the same titers, 5E+11 vg/split-dCas9/mouse. Mice were harvested at week 4. A >6-fold activation of *Afp* was observed with the additional VP64 domain. (n = 4; error bars are SEM; Student's t test; p = 0.0271). (C) To determine the *in vivo* kinetics of CRISPR activation, C57BL/6J mice were injected with 5E+11 vg/split-dCas9/mouse of AAV8 split-VP64-dCas9-VR-Afp and were bled weekly. Control mice received non-targeting AAV8 virus at the same titers, 5E+11 vg/split-dCas9/mouse. *Afp* concentrations were calculated based on *Afp* protein standard curve. *Afp* concentration peaked at week 6, at ∼19.2 ng/mL compared to a baseline of ∼3.8 ng/mL, showing a ∼5-fold increase in *Afp* concentration. (n = 6; error bars are SEM; two-way ANOVA with Dunnett's multiple comparisons post hoc test). (D) Domain and guide RNA optimization for AAV-CRISPR repression is shown: activity of multiple C-terminal domain fusions: KRAB, DNA methyltransferase (DNMT3A or DNMT3L), and FOG1 were evaluated; however, no significant additional repression in transient repression assays was observed. Higher repression was observed when utilizing two gRNAs. (n = 3; error bars are SEM; HEK293T cells; locus: *CXCR4*). *p ≤ 0.05; **p ≤ 0.01; ***p ≤ 0.001 ****p ≤ 0.0001.

mCAR- and mOpsin-positive cells (Figures S3E and S3F). Taken together, the above experiments confirmed the efficacy of our dual-AAV-CRISPR platform in engineering *in situ* cellular reprogramming of retinal rod cells.

Prevention of Photoreceptor Degeneration in a Retinitis Pigmentosa Mouse Model

Next, to validate our approach in a retinitis pigmentosa mouse model, we targeted *Nrl* in rd10 mice, a model of autosomal recessive retinitis
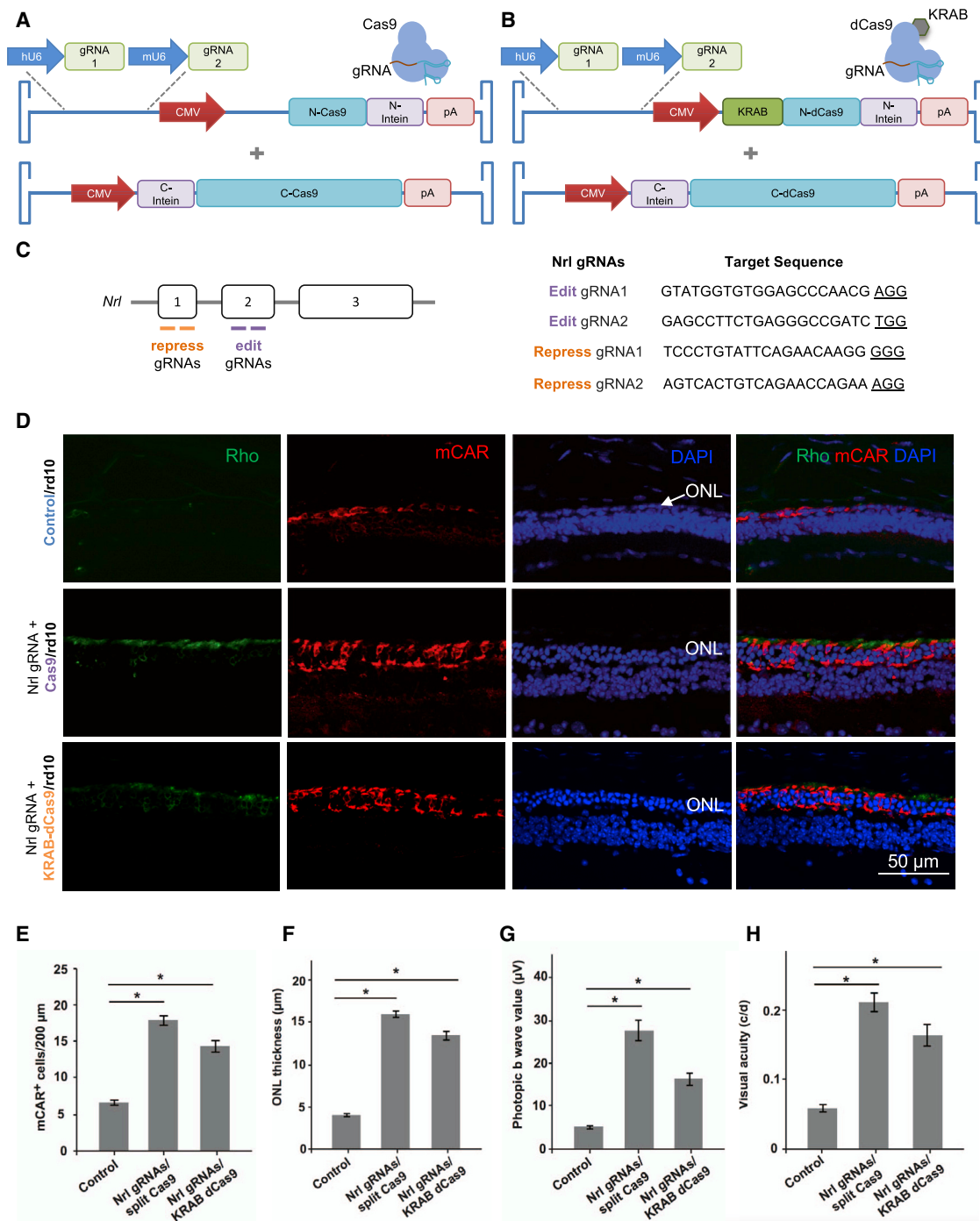
Figure 3. Dual-AAV Split-dCas9 Repression Strategy Rescues Retinal Function in rd10 Mice

(A) Schematic of AAV construction for split-Cas9-Nrl gene editing vectors. To avoid repeat sequences in the AAV, a human U6 promoter and a mouse U6 promoter were utilized to drive each individual gRNA. (B) Approach for modular usage of effector cassettes to enable genome repression via a split-KRAB-dCas9-Nrl repressor is shown. (C) Target sequences for *Nrl* genome editing and repression are shown. PAM sequences are underlined. (D) Immunofluorescence analysis of mCAR^{+} cells in rd10 mouse retina treated with AAV-split-Cas9-Nrl or AAV-split-KRAB-dCas9-Nrl is shown. Mice were treated at P7 and harvested at P50. Rhodopsin, green; mCAR, red; DAPI, blue. (E) Quantification of mCAR^{+} cells in rd10 mice retina treated with AAV-split-Cas9-Nrl or AAV-split-KRAB-dCas9-Nrl is shown. Results are shown as mean ± SEM. (*p < 0.05;

(legend continued on next page)

pigmentosa. These mice carry a spontaneous mutation of the rod-phosphodiesterase gene and exhibit rod degeneration around P18. By P60, rods are no longer detectable, with accompanying cone photoreceptor degeneration.[53] To assess whether conversion of rods to cones is sufficient to reverse degeneration and rescue visual function, we subretinally injected split-Cas9-Nrl or split-KRAB-dCas9-Nrl in rd10 mice at P7. Whereas untreated eyes had sparsely distributed photoreceptor cell nuclei in the outer nuclear layer (ONL), split-Cas9-Nrl- or split-KRAB-dCas9-Nrl-treated eyes had ~2 or 3 layers of ONL, indicating that the treatment prevented photoreceptor degeneration and preserved ONL (Figures 3D–3H). To determine the effect of the treatment on cone physiological function and visual acuity, we also measured optic kinetic nystagmus (OKN) to quantify visual acuity 6 weeks after injection (P50). All eyes treated with split-KRAB-dCas9-Nrl had improved visual function, as indicated by significantly higher visual acuity (Figure 3H). Taken together, our split-KRAB-dCas9 AAV system thus paves the way for fine control of *in situ* gene expression for gene therapy of retinitis pigmentosa and importantly also enables a scarless approach for *in vivo* genome engineering.

DISCUSSION

Collectively, our integrated AAV-CRISPR delivery platform provides a facile and robust method to edit and regulate the expression of endogenous genes via Cas9- and dCas9-based effectors. In recent work, others and we have demonstrated the use of AAV-split-Cas9s.[29,30] Here, we establish a modular vector architecture whereby we also couple dCas9 and several transcriptional regulators with ease, thereby engineering the full spectrum of genome editing and regulation (both activation and repression) functionalities. This system has several advantages, including the utilization of a split-Cas9 system, which due to the limited cargo capacity of AAVs (~4.7 kb) is an optimal approach to enable desired genome engineering applications. Additionally, one can utilize desired accessory elements of interest to optimize transcription of the payloads. We show that our AAV-CRISPR system can be utilized to achieve a high level of *in vivo* transcriptional repression (up to 80%; Figure 1D) and *in vivo* transcriptional activation (up to 6-fold increase; Figure 2C), as well as for editing *in vitro* in HEK293T cells and CD34+ hematopoietic stem cells (HSCs) and *in vivo* in C57BL/6J mice (Figure S1).

Furthermore, we demonstrated for the first time the utility of AAV-KRAB-dCas9-mediated *in situ* gene repression in the context of gene therapy, specifically to prevent vision loss in a mouse model of retinitis pigmentosa (rd10 mice; Figure 3). With our approach, we demonstrate reprogramming of rod to cone-like cell fate, with rescue of visual function, by targeted inactivation or repression of *Nrl*. Gene targeting efficiency was significantly improved with our dual-gRNA strategy. Using our cellular reprogramming approach, we demonstrate significant rescue and preservation of cone function. However, this approach may also reduce rod photoreceptor number and function and therefore lead to night blindness. Nonetheless, studies have indicated that retinitis pigmentosa patients are willing to tolerate night blindness, as it is considered an acceptable risk given the potential for significant restoration of cone function and therefore of daylight vision. Furthermore, as retinitis pigmentosa in advanced stages of the disease eventually leads to loss of both rods and cones, and therefore to legal blindness, this reprogramming strategy would represent an attractive therapeutic approach.

We note that secondary cone degeneration and death in retinitis pigmentosa may be due to toxic factors released from dying rods that damage cones or to an unfavorable environment from ONL collapse that cannot maintain sufficient structural or physiological support for cones. It can be hypothesized that the preservation of rod cell bodies may thus provide the requisite support necessary to prevent secondary cone death. Indeed, $Gnat1^{-/-}$ knockout mice, which have severe rod dysfunction, have cones with near normal histology and function without significant rod degeneration or ONL collapse.[54,55] In fact, our current study showed increased ONL thickness in eyes treated with AAV-split-Cas9-Nrl and AAV-split-KRAB-dCas9-Nrl. Moving forward, it will, however, be important to perform long-term studies in the mice to determine the effects of prolonged *Nrl* repression. As such, an advantage of using a repression-based system via the dual AAV-split-KRAB-dCas9 is that this strategy provides a potentially reversible approach for gene therapy, with no risk of mutagenesis due to the inactivation of the Cas9 nuclease activity.[12,15] In addition, recessive mutations in *NRL* can cause retinal degeneration, which is why an *in vivo* gene repression (versus gene editing) of *Nrl* to rescue cone degeneration is advantageous given the deleterious long-term effects of *Nrl* ablation.

An additional advantage of utilizing this system is that one can also potentially multiplex gene activation or repression,[56] which could be beneficial for complex diseases that have multiple loci involved. Additionally, genes that are typically difficult to edit could also be readily accessed through the dCas9 system. Finally, because dCas9 lacks endonuclease activity, and there is no permanent change to the genome, off-target effects that can lead to oncogenesis can also be avoided. We also note some potential limitations of our system: utilizing a split-Cas9 system will have reduced targeting efficiency as both components, CCas9 and NCas9, have to be co-delivered to the target cell of interest to reconstitute Cas9 activity. Additionally, because dCas9 does not enable a permanent change to the genome, multiple treatments might be necessary. We, however, expect that, with steady improvements in techniques for localized tissue-specific delivery and optimization of AAV production, these aspects will be progressively addressed.

Student's t test; n = 3). (F) Increased ONL thickness in rd10 mice retina treated with AAV-split-Cas9-Nrl and AAV-split-KRAB-dCas9-Nrl is shown. ONL, outer nuclear layer. Results are shown as mean ± SEM. (*p < 0.05; Student's t test; n = 3). (G) Quantification of b wave amplitude in AAV-split-Cas9-Nrl and AAV-split-KRAB-dCas9-Nrl injected and uninjected rd10 mice is shown. Results are shown as mean ± SEM. (*p < 0.05; paired Student's t test; n = 3). (H) Quantification of visual acuity in rd10 mouse retina treated with AAV-split-Cas9-Nrl and AAV-split-KRAB-dCas9-Nrl is shown. Results are shown as mean ± SEM. (*p < 0.05; Student's t test; n = 3).

Taken together, we believe that our CRISPR-dCas9-mediated *in situ* cellular reprogramming approach represents a promising strategy in the prevention of tissue degradation and restoration of normal tissue function and points to an important approach toward the treatment of human diseases in a gene- and mutation-independent context. We also anticipate our programmable multi-functional AAV-based synthetic delivery platform, through its ready programmability in CRISPR effector incorporation, will have broad utility in basic science and translational applications.

MATERIALS AND METHODS
Vector Design and Construction
See Supplemental Notes for annotated sequence information on the modules used for the AAV vector constructions. Split-Cas9/dCas9 AAV vectors were constructed by sequential assembly of corresponding gene blocks (Integrated DNA Technologies) into a custom synthesized rAAV2 vector backbone. gRNA sequences were inserted into NCas9 or dNCas9 plasmids by cloning oligonucleotides (IDT) encoding spacers into AgeI cloning sites via Gibson assembly.

gRNA Designs
Editing gRNAs were designed utilizing the *in silico* tool: MIT CRISPR Design and Broad Institute CRISPRko (https://portals.broadinstitute.org/gpp/public/analysis-tools/sgrna-design). Regulation gRNAs were designed utilizing an *in silico* tool to predict gRNAs.[57]

Mammalian Cell Culture
All HEK293T cells were grown in DMEM (10%) supplemented with 10% fetal bovine serum (FBS) and 1% Antibiotic-Antimycotic (Thermo Fisher Scientific) in an incubator at 37°C and 5% CO_2 atmosphere. HEK293T cells were plated in 24-well plates for AAV transductions. Hematopoietic stem cells expressing CD34 (CD34+ cells) were grown in serum-free StemSpan SFEM II with StemSpan CD34+ Expansion Supplement (10×; all from STEMCELL Technologies). CD34+ cells were plated in 96-well plates for AAV transductions.

Production of AAVs
AAV8 was utilized for *in vivo* studies in the liver, AAV2-Y444F was used for *in situ* studies in the eye, AAV6 was utilized for *in vitro* studies in CD34+ cells, and AAV-DJ was utilized for *in vitro* studies in HEK293T cells.

Large-Scale Production
Virus was either prepared by the Gene Transfer, Targeting and Therapeutics (GT3) core at the Salk Institute of Biological Studies (La Jolla, CA) or in house utilizing the GT3 core protocol. Briefly, AAV2/8, AAV2/2-Y444F, AAV2/6, and AAV2/DJ virus particles were produced using HEK293T cells via the triple transfection method and purified via an iodixanol gradient.[58] Confluency at transfection was between 80% and 90%. Media was replaced with pre-warmed media 2 hr before transfection. Each virus was produced in 5 × 15 cm plates, where each plate was transfected with 7.5 μg of pXR-capsid (pXR-8, pXR-2-Y444F, pXR-6, and pXR-DJ), 7.5 of μg recombinant transfer

vector, and 22.5 μg of pAd5 helper vector using polyethylenimine (PEI; 1 μg/μL linear PEI in 1×DPBS [pH 4.5], using HCl) at a PEI:DNA mass ratio of 4:1. The mixture was incubated for 10 min at room temperature and then applied dropwise onto the media. The virus was harvested after 72 hr and purified using an iodixanol density gradient ultracentrifugation method. The virus was then dialyzed with 1× PBS (pH 7.2) supplemented with 50 mM NaCl and 0.0001% of Pluronic F68 (Thermo Fisher Scientific) using 100-kDa filters (Millipore) to a final volume of ~1 mL and quantified by qPCR using primers specific to the ITR region, against a standard (ATCC VR-1616): AAV-ITR-F: 5′-CGGCCTCAGTGAGCGA-3′ and AAV-ITR-R: 5′-GGAACCCCTAGTGATGGAGTT-3′.

Small-Scale Production
Small-scale AAV preps were prepared using 6-well plates containing HEK293T cells, which were co-transfected with 0.5 μg pXR-capsid, 0.5 μg recombinant transfer vector, and 1.5 μg pAd5 helper vector using PEI. The cells and supernatant were harvested after 72 hr, and the crude extract was utilized to transduce HEK293T cells in 24-well plates. Small-scale production virus was utilized to generate data from Figures 1C, 1E, S1C, and S1D.

Lipid-Mediated Cell Transfections
One day prior to transfection, HEK293T cells were seeded in a 24-well plate at a cell density of 1 or 2E+5 cells per well. 0.5 μg of each plasmid was added to 25 μL of Opti-MEM medium, followed by addition of 25 μL of Opti-MEM containing 2 μL of Lipofectamine 2000. The mixture was incubated at room temperature for 15 min and then added to the cells. The entire solution was added to the cells in a 24-well plate and mixed by gently swirling the plate. Media was changed after 24 hr, and the plate was incubated at 37°C for 72 hr in a 5% CO_2 incubator. Cells were harvested, spun down, and frozen at −80°C.

T7E1 Assay
To examine the efficacy of the *Nrl* gRNAs, we performed T7E1 assay in immortalized mouse fibroblasts. Briefly, cells were transfected with pAAV-U6-gRNA and hCas9 (Addgene 41815) using Lipofectamine 2000 (Thermo Fisher Scientific). Two days after transfection, the cells were harvested and genomic DNA was extracted with DNeasy Blood & Tissue kit (QIAGEN), and a T7E1 (New England Biolabs) assay was done following manufacturer's instructions. Primers to amplify genomic regions are listed as following: NRL-F: 5′-ACCTCTCT CTGCTCAGTCCC-3′ and NRL-R: 5′-GACATGCTGGGCTCCTG TC-3′. The cleavage frequency was calculated from the proportion of cut bands intensity to total bands intensity.

Animal Experiments
AAV Injections
All animal procedures were performed in accordance with protocols approved by the Institutional Animal Care and Use Committee (IACUC) of the University of California, San Diego and adhered to the ARVO Statement for the Use of Animals in Ophthalmic and Vision Research. All mice were acquired from Jackson Laboratory.

AAV injections were done in adult C57BL/6J mice (10 weeks) through tail-vein injections using 5E+11 vg/mouse of each split-Cas9 (total virus of 1E+12 vg/mouse) or in rd10, NRL-EGFP, and C57BL/6J neonates (P7) through subretinal injections as previously described[59,60] using ~1E+10 vg/mouse of each split-Cas9 (total virus of ~2E+10). For subretinal injections, approximately 0.5 μL AAV2-Y444F was introduced into the subretinal space using a pulled angled glass pipette controlled by a FemtoJet (Eppendorf). The left eyes were uninjected for within-animal controls. Experimental mice were anesthetized with an intraperitoneal injection of a mixture of ketamine and xylazine. Pupils were dilated with 1% topical tropicamide. Subretinal injection was performed under direct visualization using a dissecting and a glass micropipette (internal diameter 50~75 μm). A successful injection was judged by creation of a small subretinal fluid bleb. Fundus examination was performed immediately following injection, and mice showing any sign of retinal damage, such as bleeding, were excluded from final animal counts.

Doxycycline Administration
Mice transduced with pAAV inducible-Cas9 vectors were given intraperitoneal (i.p.) injections of 200 mg doxycycline in 10 mL 0.9% NaCl with 0.4 mL of 1N HCl three times a week for four weeks.

OKN Tests
Visual acuity testing of all animals was conducted at 5 weeks after injection with an optomotor testing apparatus as previously reported.[61] Briefly, a virtual reality chamber was created with four computer monitors facing into a square. A virtual cylinder, covered with a vertical sine wave grating, was drawn and projected onto the monitors using software running on a Java application. The animal was placed on a platform within a clear cylinder (diameter ~30 cm) in the center of the square. A video camera situated above the animal provided real-time video feedback on another computer screen. From the mouse's point of view, the monitors appeared as large windows through which the animals viewed the rotating cylinder. Each mouse was placed on the platform in a quiet environment before the test until it became accustomed to the test conditions with minimal movement. The virtual stripe cylinder was set up at the highest level of contrast (100%; black 0; white 255; illuminated from above 250 cd/m^2), with the number of stripes starting from 4 per screen (2 black and 2 white). The test began with 1 min of clockwise rotation at a speed of 13. (The baseline value is 10, at which the bars move 1 pixel/cycle. Values less than 10 delay the cycle by X × 100 ms, with a minimum value of 1). An unbiased observer tracked and recorded the head movements of the mouse. The test was then repeated with 1 min of counterclockwise rotation. The data were measured by cycles/degree (c/d) and expressed as mean ± SEM with comparison using a t test statistical analysis. A p value < 0.05 was considered statistically significant.

Histology
Mice were humanely sacrificed by CO_2. Eyeballs were dissected, marked with the injection site, and fixed in 4% paraformaldehyde (PFA). Cornea, lens, and vitreous were removed from each eye without disturbing the retina. The remaining retina-containing eyecup was infiltrated with 30% sucrose and embedded in optimal cutting temperature (OCT) compound. Horizontal frozen sections were cut on a cryostat. Care was taken to obtain retinal sections from control and experimental groups along comparable points along the dorsal-ventral axis. Retinal cross-sections were prepared for histological evaluation by immunofluorescence staining.

Immunofluorescence
Retinal cryosections were rinsed in PBS and blocked in 0.5% Triton X-100 and 5% BSA in PBS for 1 hr at room temperature, followed by an overnight incubation in primary antibodies at 4°C. After three washes in PBS, sections were incubated with secondary antibody. Cell nuclei were counterstained with DAPI. The following antibodies were used: mouse anti-rhodopsin monoclonal antibody (Abcam; ab3267); rabbit anti-opsin polyclonal antibody (Millipore; AB5405); and rabbit anti-cone arrestin polyclonal antibody (Millipore; AB15282). The following secondary antibodies, Alexa-488- or Alexa-Fluor-555-conjugated anti-mouse or rabbit immunoglobulin G (IgG) (Invitrogen) were used at a dilution of 1:500. Sections were mounted with Fluoromount-G (Southern Biotech) and coverslipped. Images were captured using Olympus FV1000 confocal microscope.

Gene Expression Analysis and qRT-PCR
RNA from cells was extracted using RNeasy kit (QIAGEN; 74104), from liver using RNeasy Plus Universal Kit (QIAGEN; 73442), and from eyeballs using AllPrep DNA/RNA Mini Kit (QIAGEN; 80204). cDNA was synthesized from RNA using Protoscript II Reverse Transcriptase Kit (NEB; E6560L). Real-time PCR (qPCR) reactions were performed using the KAPA SYBR Fast qPCR Kit (Kapa Biosystems; KK4601), with gene-specific primers (Table S2A) in technical triplicates and in biological triplicates. Relative mRNA expression was calculated using the comparative CT (ΔΔCT) method and normalized to β-actin or GAPDH. Mean fold change and SD were calculated using Microsoft Excel.

Genomic DNA Extraction and NGS Preps
Genomic DNA from cells and tissues was extracted using DNeasy Blood and Tissue Kit (QIAGEN; 69504), according to the manufacturer's protocol. Next-generation sequencing libraries were prepared as follows. Briefly, 4–10 μg of input whole-liver gDNA was amplified by PCR with primers that amplify 150 bp surrounding the sites of interest (Table S2B) using KAPA Hifi HotStart PCR Mix (Kapa Biosystems; KK2602). PCR products were gel purified (QIAGEN; 28704) and further purified (QIAGEN PCR Purification Kit; 28104) to eliminate byproducts. Library construction was done with NEBNext Multiplex Oligos for Illumina kit (NEB; E7335S). 10–25 ng of input DNA was amplified with indexing primers. Samples were then purified and quantified using a qPCR library quantification kit (Kapa Biosystems; KK4824). Samples were then pooled and loaded on an Illumina Miseq (150 bp paired-end run or 150 single-end run) at 4 nM concentrations. Data analysis was performed using CRISPR Genome Analyzer.[40]

ELISA

Levels of serum *Afp* were measured using the alpha-fetoprotein (Afp) mouse ELISA kit (Abcam; ab210905) according to manufacturer's guidelines. First, 50 μL of 2 μg/mL capture antibody was added to each well of a 96-well of a high bind microplate (ab210903). The plates were sealed and incubated overnight at 4°C on a plate rocker. The plates were manually washed three times with 350 μL of 1× wash buffer (ab206977). To reduce non-specific binding, the plates were blocked by adding 300 μL of 1× blocking buffer (ab210904) to each well. The plates were then sealed and incubated at room temperature for 2 hr. Plates were washed as described above. The Afp protein standards were diluted in 1× blocking buffer (ab210904) and prepared for a two-fold diluted standard curve. Samples were diluted 1:20 in 1× blocking buffer (ab210904), and 50 μL of sample and standard (in duplicates) were added onto the plates and allowed to bind for 2 hr. Plates were washed as described above. Then, 50 μL of 0.5 μg/mL of detector antibody was added to each well and incubated for 1 hr at room temperature. The plates were washed as described above. Horseradish peroxidase (HRP)-streptavidin solution (ab20901) was added to each well at a 1:7,500 dilution and incubated at room temperature for 1 hr. Plates were washed as described above. Then, 100 μL of 3,3′,5,5′-tetramethylbenzidine (TMB) substrate was added to each well and incubated until optimal blue density was obtained. Finally, 100 μL of stop solution was added to each well. The absorbance was immediately determined on a microplate reader (BioRad iMark) at a wavelength of 450 nm.

SUPPLEMENTAL INFORMATION

Supplemental Information includes Supplemental Notes, three figures, and two tables and can be found with this article online at https://doi.org/10.1016/j.ymthe.2018.04.017.

AUTHOR CONTRIBUTIONS

A.M.M., K.Z., and P.M. designed the study. A.M.M., D.K., J.M., J.C., J.T., J.N., and P.M. performed experiments and viral productions toward the *in vitro* and *in vivo* studies to engineer and characterize the gene targeting systems. X.F. and J.Z. performed and X.F., J.Z., and K.Z. analyzed all retina gene targeting studies. L.L., Y.-R.V.S., and S.V. provided technical advice. A.M.M., K.Z., and P.M. wrote the manuscript.

CONFLICTS OF INTEREST

The authors declare no conflict of interest.

ACKNOWLEDGMENTS

REFERENCES

1. Charpentier, E., and Doudna, J.A. (2013). Biotechnology: rewriting a genome. Nature 495, 50–51.

2. Hwang, W.Y., Fu, Y., Reyon, D., Maeder, M.L., Tsai, S.Q., Sander, J.D., Peterson, R.T., Yeh, J.R., and Joung, J.K. (2013). Efficient genome editing in zebrafish using a CRISPR-Cas system. Nat. Biotechnol. 31, 227–229.

3. Li, D., Qiu, Z., Shao, Y., Chen, Y., Guan, Y., Liu, M., Li, Y., Gao, N., Wang, L., Lu, X., et al. (2013). Heritable gene targeting in the mouse and rat using a CRISPR-Cas system. Nat. Biotechnol. 31, 681–683.

4. Mali, P., Esvelt, K.M., and Church, G.M. (2013). Cas9 as a versatile tool for engineering biology. Nat. Methods 10, 957–963.

5. Mali, P., Yang, L., Esvelt, K.M., Aach, J., Guell, M., DiCarlo, J.E., Norville, J.E., and Church, G.M. (2013). RNA-guided human genome engineering via Cas9. Science 339, 823–826.

6. Nakayama, T., Fish, M.B., Fisher, M., Oomen-Hajagos, J., Thomsen, G.H., and Grainger, R.M. (2013). Simple and efficient CRISPR/Cas9-mediated targeted mutagenesis in Xenopus tropicalis. Genesis 51, 835–843.

7. Zhang, X.-H., Tee, L.Y., Wang, X.-G., Huang, Q.-S., and Yang, S.-H. (2015). Off-target effects in CRISPR/Cas9-mediated genome engineering. Mol. Ther. Nucleic Acids 4, e264.

8. Shan, Q., Wang, Y., Li, J., Zhang, Y., Chen, K., Liang, Z., Zhang, K., Liu, J., Xi, J.J., Qiu, J.L., and Gao, C. (2013). Targeted genome modification of crop plants using a CRISPR-Cas system. Nat. Biotechnol. 31, 686–688.

9. Yang, D., Xu, J., Zhu, T., Fan, J., Lai, L., Zhang, J., and Chen, Y.E. (2014). Effective gene targeting in rabbits using RNA-guided Cas9 nucleases. J. Mol. Cell Biol. 6, 97–99.

10. Yu, Z., Ren, M., Wang, Z., Zhang, B., Rong, Y.S., Jiao, R., and Gao, G. (2013). Highly efficient genome modifications mediated by CRISPR/Cas9 in Drosophila. Genetics 195, 289–291.

11. DiCarlo, J.E., Norville, J.E., Mali, P., Rios, X., Aach, J., and Church, G.M. (2013). Genome engineering in Saccharomyces cerevisiae using CRISPR-Cas systems. Nucleic Acids Res. 41, 4336–4343.

12. Qi, L.S., Larson, M.H., Gilbert, L.A., Doudna, J.A., Weissman, J.S., Arkin, A.P., and Lim, W.A. (2013). Repurposing CRISPR as an RNA-guided platform for sequence-specific control of gene expression. Cell 152, 1173–1183.

13. Chavez, A., Scheiman, J., Vora, S., Pruitt, B.W., Tuttle, M., P R Iyer, E., Lin, S., Kiani, S., Guzman, C.D., Wiegand, D.J., et al. (2015). Highly efficient Cas9-mediated transcriptional programming. Nat. Methods 12, 326–328.

14. Hilton, I.B., D'Ippolito, A.M., Vockley, C.M., Thakore, P.I., Crawford, G.E., Reddy, T.E., and Gersbach, C.A. (2015). Epigenome editing by a CRISPR-Cas9-based acetyl-transferase activates genes from promoters and enhancers. Nat. Biotechnol. 33, 510–517.

15. Mali, P., Aach, J., Stranges, P.B., Esvelt, K.M., Moosburner, M., Kosuri, S., Yang, L., and Church, G.M. (2013). CAS9 transcriptional activators for target specificity screening and paired nickases for cooperative genome engineering. Nat. Biotechnol. 31, 833–838.

16. Maeder, M.L., Linder, S.J., Cascio, V.M., Fu, Y., Ho, Q.H., and Joung, J.K. (2013). CRISPR RNA-guided activation of endogenous human genes. Nat. Methods 10, 977–979.

17. Niu, Y., Shen, B., Cui, Y., Chen, Y., Wang, J., Wang, L., Kang, Y., Zhao, X., Si, W., Li, W., et al. (2014). Generation of gene-modified cynomolgus monkey via Cas9/RNA-mediated gene targeting in one-cell embryos. Cell 156, 836–843.

18. Su, S., Hu, B., Shao, J., Shen, B., Du, J., Du, Y., Zhou, J., Yu, L., Zhang, L., Chen, F., et al. (2016). CRISPR-Cas9 mediated efficient PD-1 disruption on human primary T cells from cancer patients. Sci. Rep. 6, 20070.

19. Yin, H., Song, C.-Q., Dorkin, J.R., Zhu, L.J., Li, Y., Wu, Q., Park, A., Yang, J., Suresh, S., Bizhanova, A., et al. (2016). Therapeutic genome editing by combined viral and non-viral delivery of CRISPR system components in vivo. Nat. Biotechnol. 34, 328–333.

20. Yin, H., Xue, W., Chen, S., Bogorad, R.L., Benedetti, E., Grompe, M., Koteliansky, V., Sharp, P.A., Jacks, T., and Anderson, D.G. (2014). Genome editing with Cas9 in adult mice corrects a disease mutation and phenotype. Nat. Biotechnol. *32*, 551–553.

21. Zuris, J.A., Thompson, D.B., Shu, Y., Guilinger, J.P., Bessen, J.L., Hu, J.H., Maeder, M.L., Joung, J.K., Chen, Z.Y., and Liu, D.R. (2015). Cationic lipid-mediated delivery of proteins enables efficient protein-based genome editing in vitro and in vivo. Nat. Biotechnol. *33*, 73–80.

22. Xu, L., Park, K.H., Zhao, L., Xu, J., El Refaey, M., Gao, Y., Zhu, H., Ma, J., and Han, R. (2016). CRISPR-mediated genome editing restores dystrophin expression and function in mdx mice. Mol. Ther. *24*, 564–569.

23. Ran, F.A., Cong, L., Yan, W.X., Scott, D.A., Gootenberg, J.S., Kriz, A.J., Zetsche, B., Shalem, O., Wu, X., Makarova, K.S., et al. (2015). In vivo genome editing using Staphylococcus aureus Cas9. Nature *520*, 186–191.

24. Long, C., Amoasii, L., Mireault, A.A., McAnally, J.R., Li, H., Sanchez-Ortiz, E., Bhattacharyya, S., Shelton, J.M., Bassel-Duby, R., and Olson, E.N. (2016). Postnatal genome editing partially restores dystrophin expression in a mouse model of muscular dystrophy. Science *351*, 400–403.

25. Tabebordbar, M., Zhu, K., Cheng, J.K.W., Chew, W.L., Widrick, J.J., Yan, W.X., Maesner, C., Wu, E.Y., Xiao, R., Ran, F.A., et al. (2016). In vivo gene editing in dystrophic mouse muscle and muscle stem cells. Science *351*, 407–411.

26. Nelson, C.E., Hakim, C.H., Ousterout, D.G., Thakore, P.I., Moreb, E.A., Rivera, R.M.C., Madhavan, S., Pan, X., Ran, F.A., Yan, W.X., et al. (2016). In vivo genome editing improves muscle function in a mouse model of Duchenne muscular dystrophy. Science *351*, 403–407.

27. Kotterman, M.A., Chalberg, T.W., and Schaffer, D.V. (2015). Viral vectors for gene therapy: translational and clinical outlook. Annu. Rev. Biomed. Eng. *17*, 63–89.

28. Mingozzi, F., and High, K.A. (2013). Immune responses to AAV vectors: overcoming barriers to successful gene therapy. Blood *122*, 23–36.

29. Chew, W.L., Tabebordbar, M., Cheng, J.K.W., Mali, P., Wu, E.Y., Ng, A.H.M., Zhu, K., Wagers, A.J., and Church, G.M. (2016). A multifunctional AAV-CRISPR-Cas9 and its host response. Nat. Methods *13*, 868–874.

30. Truong, D.-J.J., Kühner, K., Kühn, R., Werfel, S., Engelhardt, S., Wurst, W., and Ortiz, O. (2015). Development of an intein-mediated split-Cas9 system for gene therapy. Nucleic Acids Res. *43*, 6450–6458.

31. Wright, A.V., Sternberg, S.H., Taylor, D.W., Staahl, B.T., Bardales, J.A., Kornfeld, J.E., and Doudna, J.A. (2015). Rational design of a split-Cas9 enzyme complex. Proc. Natl. Acad. Sci. USA *112*, 2984–2989.

32. Zetsche, B., Volz, S.E., and Zhang, F. (2015). A split-Cas9 architecture for inducible genome editing and transcription modulation. Nat. Biotechnol. *33*, 139–142.

33. Hartong, D.T., Berson, E.L., and Dryja, T.P. (2006). Retinitis pigmentosa. Lancet *368*, 1795–1809.

34. Hamel, C. (2006). Retinitis pigmentosa. Orphanet J. Rare Dis. *1*, 40.

35. Montana, C.L., Kolesnikov, A.V., Shen, S.Q., Myers, C.A., Kefalov, V.J., and Corbo, J.C. (2013). Reprogramming of adult rod photoreceptors prevents retinal degeneration. Proc. Natl. Acad. Sci. USA *110*, 1732–1737.

36. Cheng, H., Khanna, H., Oh, E.C.T., Hicks, D., Mitton, K.P., and Swaroop, A. (2004). Photoreceptor-specific nuclear receptor NR2E3 functions as a transcriptional activator in rod photoreceptors. Hum. Mol. Genet. *13*, 1563–1575.

37. Yu, W., Mookherjee, S., Chaitankar, V., Hiriyanna, S., Kim, J.-W., Brooks, M., Ataeijannati, Y., Sun, X., Dong, L., Li, T., et al. (2017). Nrl knockdown by AAV-delivered CRISPR/Cas9 prevents retinal degeneration in mice. Nat. Commun. *8*, 14716.

38. Zhu, J., Ming, C., Fu, X., Duan, Y., Hoang, D.A., Rutgard, J., Zhang, R., Wang, W., Hou, R., Zhang, D., et al. (2017). Gene and mutation independent therapy via CRISPR-Cas9 mediated cellular reprogramming in rod photoreceptors. Cell Res. *27*, 830–833.

40. Güell, M., Yang, L., and Church, G.M. (2014). Genome editing assessment using CRISPR Genome Analyzer (CRISPR-GA). Bioinformatics *30*, 2968–2970.

41. Davis, K.M., Pattanayak, V., Thompson, D.B., Zuris, J.A., and Liu, D.R. (2015). Small molecule-triggered Cas9 protein with improved genome-editing specificity. Nat. Chem. Biol. *11*, 316–318.

42. Nguyen, D.P., Miyaoka, Y., Gilbert, L.A., Mayerl, S.J., Lee, B.H., Weissman, J.S., Conklin, B.R., and Wells, J.A. (2016). Ligand-binding domains of nuclear receptors facilitate tight control of split CRISPR activity. Nat. Commun. *7*, 12009.

44. Farzadfard, F., Perli, S.D., and Lu, T.K. (2013). Tunable and multifunctional eukaryotic transcription factors based on CRISPR/Cas. ACS Synth. Biol. *2*, 604–613.

45. Gilbert, L.A., Larson, M.H., Morsut, L., Liu, Z., Brar, G.A., Torres, S.E., Stern-Ginossar, N., Brandman, O., Whitehead, E.H., Doudna, J.A., et al. (2013). CRISPR-mediated modular RNA-guided regulation of transcription in eukaryotes. Cell *154*, 442–451.

46. Kearns, N.A., Genga, R.M., Enuameh, M.S., Garber, M., Wolfe, S.A., and Maehr, R. (2014). Cas9 effector-mediated regulation of transcription and differentiation in human pluripotent stem cells. Development *141*, 219–223.

47. Thakore, P.I., D'Ippolito, A.M., Song, L., Safi, A., Shivakumar, N.K., Kabadi, A.M., Reddy, T.E., Crawford, G.E., and Gersbach, C.A. (2015). Highly specific epigenome editing by CRISPR-Cas9 repressors for silencing of distal regulatory elements. Nat. Methods *12*, 1143–1149.

48. Amabile, A., Migliara, A., Capasso, P., Biffi, M., Cittaro, D., Naldini, L., and Lombardo, A. (2016). Inheritable silencing of endogenous genes by hit-and-run targeted epigenetic editing. Cell *167*, 219–232.e14.

49. Liu, X.S., Wu, H., Ji, X., Stelzer, Y., Wu, X., Czauderna, S., Shu, J., Dadon, D., Young, R.A., and Jaenisch, R. (2016). Editing DNA methylation in the mammalian genome. Cell *167*, 233–247.e17.

50. O'Geen, H., Ren, C., Nicolet, C.M., Perez, A.A., Halmai, J., Le, V.M., Mackay, J.P., Farnham, P.J., and Segal, D.J. (2017). dCas9-based epigenome editing suggests acquisition of histone methylation is not sufficient for target gene repression. Nucleic Acids Res. *45*, 9901–9916.

51. Shen, J.P., Zhao, D., Sasik, R., Luebeck, J., Birmingham, A., Bojorquez-Gomez, A., Licon, K., Klepper, K., Pekin, D., Beckett, A.N., et al. (2017). Combinatorial CRISPR-Cas9 screens for de novo mapping of genetic interactions. Nat. Methods *14*, 573–576.

52. Petrs-Silva, H., Dinculescu, A., Li, Q., Min, S.-H., Chiodo, V., Pang, J.-J., Zhong, L., Zolotukhin, S., Srivastava, A., Lewin, A.S., and Hauswirth, W.W. (2009). High-efficiency transduction of the mouse retina by tyrosine-mutant AAV serotype vectors. Mol. Ther. *17*, 463–471.

53. Chang, B., Hawes, N.L., Hurd, R.E., Davisson, M.T., Nusinowitz, S., and Heckenlively, J.R. (2002). Retinal degeneration mutants in the mouse. Vision Res. *42*, 517–525.

54. Calvert, P.D., Krasnoperova, N.V., Lyubarsky, A.L., Isayama, T., Nicoló, M., Kosaras, B., Wong, G., Gannon, K.S., Margolskee, R.F., Sidman, R.L., et al. (2000). Phototransduction in transgenic mice after targeted deletion of the rod transducin alpha -subunit. Proc. Natl. Acad. Sci. USA *97*, 13913–13918.

55. Miyamoto, M., Aoki, M., Hirai, K., Sugimoto, S., Kawasaki, K., and Imai, R. (2010). A nonsense mutation in Gnat1, encoding the α subunit of rod transducin, in spontaneous mouse models of retinal dysfunction. Exp. Eye Res. *90*, 63–69.

56. Zalatan, J.G., Lee, M.E., Almeida, R., Gilbert, L.A., Whitehead, E.H., La Russa, M., Tsai, J.C., Weissman, J.S., Dueber, J.E., Qi, L.S., and Lim, W.A. (2015). Engineering complex synthetic transcriptional programs with CRISPR RNA scaffolds. Cell *160*, 339–350.

57. Horlbeck, M.A., Gilbert, L.A., Villalta, J.E., Adamson, B., Pak, R.A., Chen, Y., Fields, A.P., Park, C.Y., Corn, J.E., Kampmann, M., and Weissman, J.S. (2016). Compact and highly active next-generation libraries for CRISPR-mediated gene repression and activation. eLife *5*, e19760.

58. Grieger, J.C., Choi, V.W., and Samulski, R.J. (2006). Production and characterization of adeno-associated viral vectors. Nat. Protoc. *1*, 1412–1428.

59. Matsuda, T., and Cepko, C.L. (2004). Electroporation and RNA interference in the rodent retina in vivo and in vitro. Proc. Natl. Acad. Sci. USA *101*, 16–22.

60. Wang, S., Sengel, C., Emerson, M.M., and Cepko, C.L. (2014). A gene regulatory network controls the binary fate decision of rod and bipolar cells in the vertebrate retina. Dev. Cell *30*, 513–527.

61. Luo, J., Baranov, P., Patel, S., Ouyang, H., Quach, J., Wu, F., Qiu, A., Luo, H., Hicks, C., Zeng, J., et al. (2014). Human retinal progenitor cell transplantation preserves vision. J. Biol. Chem. *289*, 6362–6371.